Inorganic Chemistry

Article

pubs.acs.org/IC

A Bifunctional Cr/Yb/Tm:$Ca_3Ga_2Ge_3O_{12}$ Phosphor with Near-Infrared Long-Lasting Phosphorescence and Upconversion Luminescence

Daqin Chen,* Yan Chen, Hongwei Lu, and Zhenguo Ji

College of Materials & Environmental Engineering, Hangzhou Dianzi University, Hangzhou, 310018, P. R. China

Supporting Information

ABSTRACT: Currently, upconversion nanocrystals and long-lasting phosphorescent particles have attracted extensive research interest for their possible applications as bioimaging probes. However, there are few reports concerning the achievement of both upconversion luminescence of lanthanide ions and long-lasting phosphorescence of transition metal ions in a sole host so far. Herein, we demonstrate a novel calcium gallium germanium garnet ($Ca_3Ga_2Ge_3O_{12}$) host where lanthanide ions such as Tm^{3+}/Yb^{3+} and transition metal ions such as Cr^{3+} can be easily incorporated through substituting the Ca^{2+} and Ga^{3+} respectively. This Cr/Yb/Tm:$Ca_3Ga_2Ge_3O_{12}$ phosphor exhibits both broadband near-infrared long-lasting phosphorescence of Cr^{3+} with an afterglow time of more than 7000 s and near-infrared to near-infrared upconversion luminescence of Tm^{3+}. Impressively, it is evidenced that the addition of Yb^{3+}/Tm^{3+} into Cr:$Ca_3Ga_2Ge_3O_{12}$ not only results in Tm^{3+} upconversion luminescence but also greatly increases Cr^{3+} afterglow time. Based on excitation/emission, three-dimensional thermoluminescence, and time-resolved luminescence spectra, the related long-lasting phosphorescence and upconversion luminescent mechanisms are systematically discussed as well.

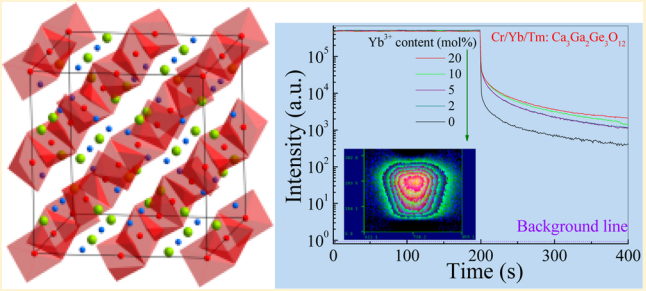

1. INTRODUCTION

Because of the growing demand for imaging tools for biomedical research and medicine, existing images systems have been rapidly improved and new techniques have been developed during the past decades.[1,2] To date, various luminescent probes, such as dye-doped particles, semiconductor quantum dots (QDs), metal nanoclusters, upconversion (UC) nanocrystals (NCs), and long-lasting phosphorescence (LLP) particles, have been used in optical imaging.[3−7]

Among them, UC NCs and LLP particles have attracted extensive research interest recently. UC is an anti-Stokes process where long wavelength exciting radiation is converted into shorter wavelength emitting light via a two-photon or multiphoton absorption mechanism.[8] Especially, lanthanide (Ln^{3+}) doped UC NCs have been developed as a new category of luminescent labels that have become promising alternatives to the organic fluorophores and quantum dots applied in biological assays and medical imaging, owing to their unique optical properties, such as low background autofluorescence, sharp emission bands, long luminescent lifetimes (micro- to milliseconds), good photostability, and low toxicity.[9−15] On the other hand, LLP is a phenomenon whereby luminescence can last for several minutes to hours after the stoppage of the excitation.[16] As a result, the long-persistent afterglow nature of LLP particles allows optical excitation before bioimaging, and permits detection and imaging without external illumination, thereby avoiding the background noise from in situ excitation.[17−21]

Moreover, it is reported that the use of near-infrared (NIR) emitting photons is more suitable for biomedical imaging and detection than that of ultraviolet (UV) or visible ones, since the "optical transmission window" of biological tissues within 700−1100 nm allows for deeper light penetration, lower autofluorescence, and reduced light scattering, resulting in increased image contrast.[22] Typically, the Tm^{3+}/Yb^{3+} couple was widely adopted to codope into an appropriate host to achieve Tm^{3+} NIR (~800 nm) UC luminescence (UCL) through energy transfer (ET) from Yb^{3+} to Tm^{3+} under 980 nm excitation (corresponding to Yb^{3+}:$^2F_{7/2}\rightarrow{}^2F_{5/2}$ transition),[23,24] while the Cr^{3+} ion is an ideal NIR LLP emitter in solid since its $3d^3$ electron configuration allows a narrow-band emission (~700 nm) due to the spin-forbidden $^2E \rightarrow {}^4A_2$ transition, or a broadband emission (650−1600 nm) ascribed to the spin-allowed $^4T_2 \rightarrow {}^4A_2$ transition, which strongly depends on the crystal-field environment of the host lattices.[25−28] In order to advance their direct applications in the multiplexed and highly sensitive bioassays, it is urgently necessary to explore optical materials with multifunctionality. Recently, persistent UC luminescence in lanthanide-doped phosphors has been demonstrated by Hyppänen and Wang et al.[29,30] However, there are few reports concerning the achievement of both NIR UCL of Tm^{3+} and NIR LLP of Cr^{3+} in a sole host so far.

Received: May 28, 2014
Published: July 28, 2014

   dx.doi.org/10.1021/ic501238u | Inorg. Chem. 2014, 53, 8638−8645

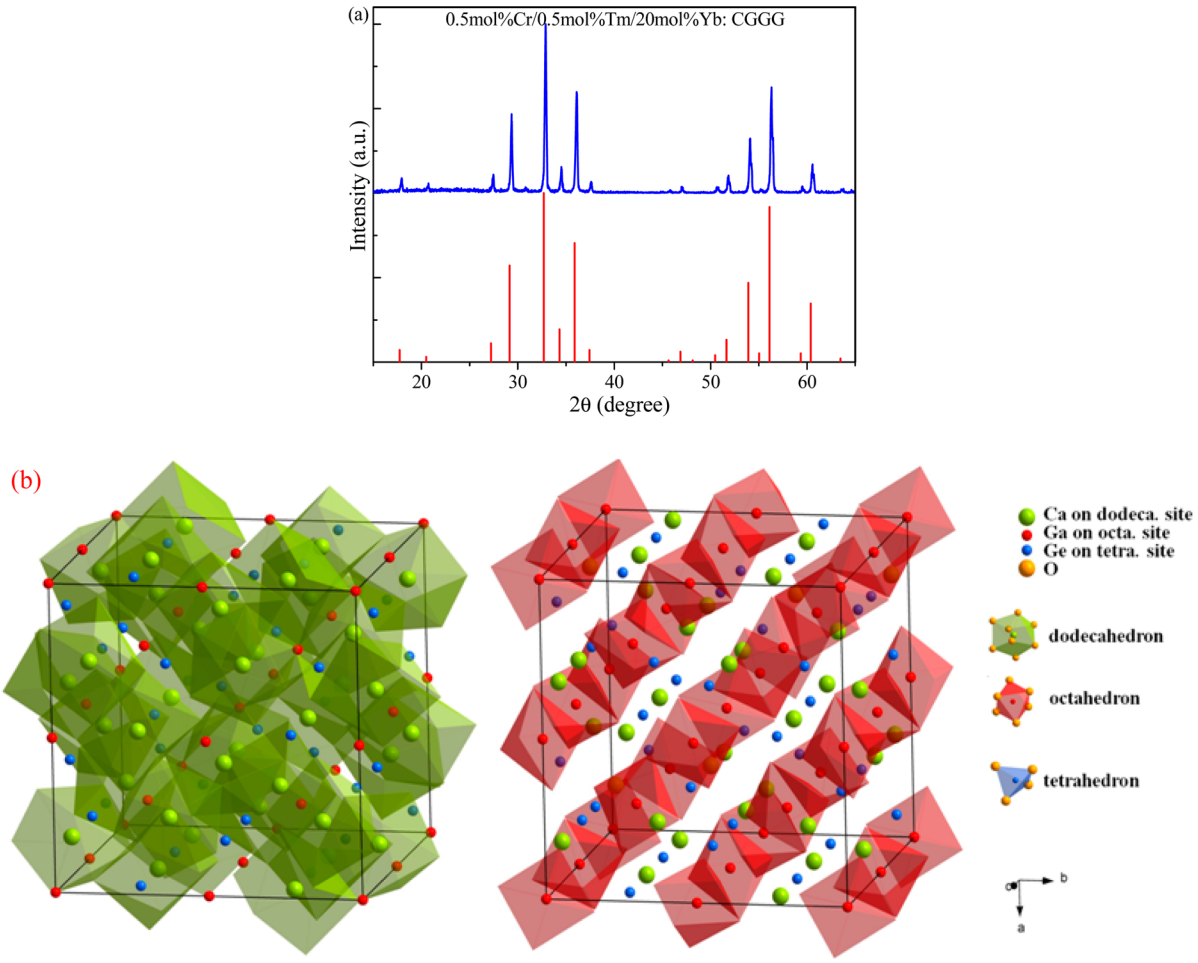

Figure 1. (a) XRD patterns of $Cr^{3+}/Tm^{3+}/Yb^{3+}$ codoped CGGG sample; bars represent standard $Ca_3Ga_2Ge_3O_{12}$ (JCPDS No. 11-0023) crystal data. (b) Unit-cell structure of CGGG (green, red, and blue spheres represent Ca^{2+}, Ga^{3+}, and Ge^{4+} on dodecahedral, octahedral, and tetrahedral sites, respectively).

Herein, $Cr^{3+}/Yb^{3+}/Tm^{3+}$ triply doped $Ca_3Ga_2Ge_3O_{12}$ (CGGG) is demonstrated to be a novel bifunctional near-infrared broadband (650−850 nm) long-lasting phosphorescence and near-infrared to near-infrared upconversion luminescence material. The selection of $Ca_3Ga_2Ge_3O_{12}$ as host for dopants is based on the easy incorporation of both lanthanide ions such as Yb^{3+}/Tm^{3+} and transition metal ions such as Cr^{3+} into the host through substituting the Ca^{2+} and Ga^{3+} respectively. Different from the case of the NIR photoluminescence (PL) of Cr^{3+} which is achieved by 250−650 nm broadband excitation, the NIR LLP could be effectively realized only by UV (250−400 nm) illumination. Notably, the addition of Yb^{3+} ions into Cr:CGGG induces the formation of extra traps because of the requirement of charge balance, which are beneficial to capturing free carriers and then immobilizing them for a long time and subsequently improving the afterglow time of Cr^{3+}. Finally, the mechanisms for NIR LLP and NIR UC luminescence in Cr/Yb/Tm:CGGG are systematically discussed based on the PL/LLP decay behaviors, the three-dimensional thermoluminescence (TL) spectra, and UCL spectra.

2. EXPERIMENTAL SECTION

Cr/Yb/Tm:$Ca_3Ga_2Ge_3O_{12}$ polycrystals were prepared by a high temperature solid-state reaction method. Stoichiometric $CaCO_3$, Ga_2O_3, GeO_2, Cr_2O_3, Tm_2O_3, and Yb_2O_3 raw materials were mixed, ground, and prefired at 900 °C for 2 h in air. After the prefired powder was finely ground again, the powder sample was calcined at 1180 °C for another 6 h in air.

X-ray diffraction (XRD) analysis with a powder diffractometer (DMAX2500 RIGAKU) using Cu Kα radiation (λ = 0.154 nm) at 40 kV and 100 mA was carried out to identify phase structure. Photoluminescence (PL), PL excitation (PLE) spectra, and luminescence decay curves in both the visible and near-infrared regions were recorded by an Edinburgh Instruments FLS920 spectrofluorometer equipped with both continuous (450 W) and pulsed xenon lamps or hydrogen lamps. Using the Hamamatsu PMT detectors (R928 and R5509-72), the visible and near-infrared luminescence signals were detected. All the measurements were carried out at room temperature.

Three-dimensional thermoluminescence spectra were recorded by using a RISΦDA-15B/C thermoluminescence/photoluminescence spectrometer. Immediately after being exposed for 10 min to an UV lamp with emission peaked at 286 nm (Gp3Hg-2, Fei Ying Light Electrical Appliance Factory), thermoluminescence signals were recorded in the temperature range of 273−773 K and the heating rate was fixed at 5 $K{\cdot}s^{-1}$.

Quantum yield (QY) is defined as the ratio of the emitted photons to the absorbed photons and was measured by a FLS920 spectrofluorometer equipped with an integrating sphere. All the recorded spectroscopic data were corrected for the spectral responses of both the spectrofluorometer and the integrating sphere. The responses of the detecting systems (integrating sphere, monochromators, and detectors) in photon flux were determined using a calibrated

dx.doi.org/10.1021/ic501238u | Inorg. Chem. 2014, 53, 8638−8645

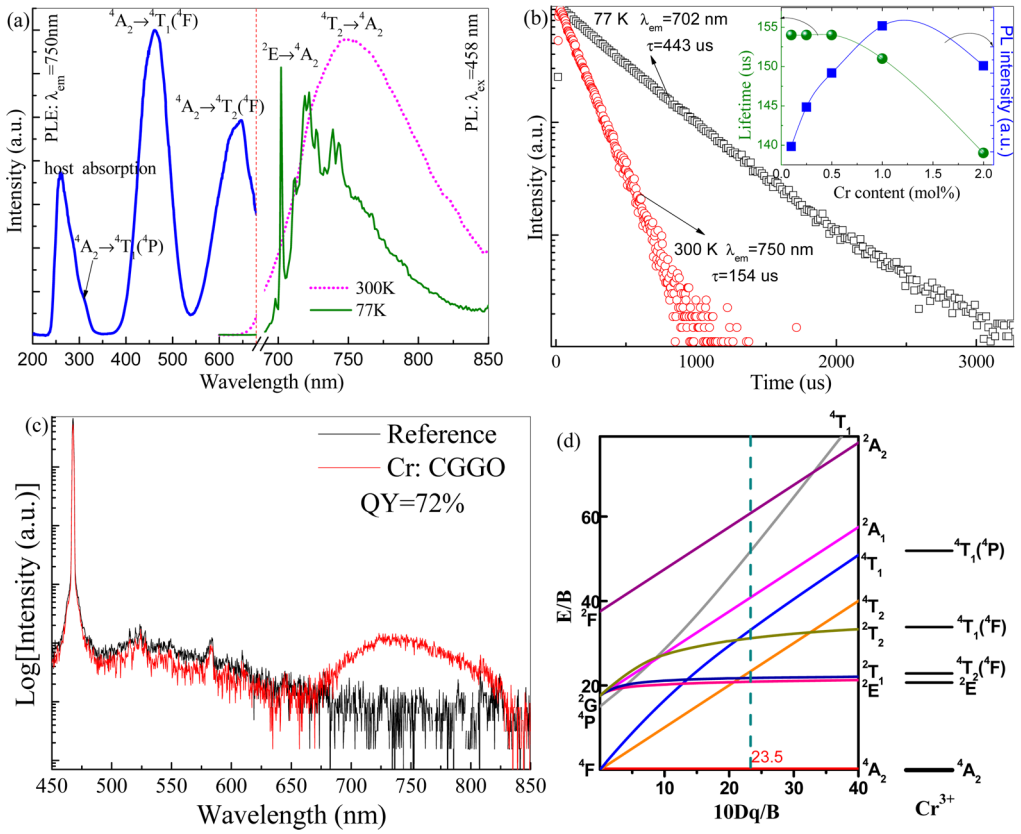

Figure 2. (a) PLE (λ_{em} = 750 nm) and PL (λ_{ex} = 458 nm) spectra of Cr:CGGG. (b) PL decay curves of Cr:CGGG monitored at 750 nm emission at RT (○) and 77 K (□); inset shows the Cr^{3+} content dependent lifetime and PL intensity of Cr:CGGG. (c) PL spectra of Cr:CGGG and reference sample recorded by a spectrofluorometer equipped with an integrating sphere for quantum yield calculation. (d) Tanabe–Sugano diagram for Cr^{3+} in CGGG.

tungsten lamp. Based on this setup, internal QY is calculated by the following equation:[31]

$$\eta = \frac{\text{no. of photons emitted}}{\text{no. of photons absorbed}} = \frac{L_{\text{sample}}}{E_{\text{reference}} - E_{\text{sample}}} \quad (1)$$

where η represents QY, L_{sample} represents the emission intensity, and $E_{\text{reference}}$ and E_{sample} represent the intensities of the excitation light not absorbed by the reference and the sample, respectively. The difference in integrated areas between the sample and the reference represents the number of the absorbed photons. The photons emitted were determined by integrating the area of the emission band. The error associated with the QY measurement is ±3%.

3. RESULTS AND DISCUSSION

As demonstrated by the XRD pattern of the as-prepared Cr^{3+}/Tm^{3+}/Yb^{3+} triply doped CGGG sample shown in Figure 1a, all the diffraction peaks are well indexed to those of the cubic $Ca_3Ga_2Ge_3O_{12}$ phase (JCPDS No. 11-0023). The doping of lanthanide and transition metal ions does not induce any other Cr^{3+}-, Tm^{3+}-, and Yb^{3+}-containing phases, indicating the successful incorporation of these activators into the CGGG host. The $Ca_3Ga_2Ge_3O_{12}$ garnet structure belongs to space group O_h^{10}-*Ia*3*d* having a unit cell showing body centered cubic symmetry with a typically large lattice parameter a = 12.252 Å.[32] The unit cell contains eight CGGG formula units, giving a total of 120 ions per unit cell. Of the 160 ions, 96 are oxygen, and it is convenient to visualize their distribution in terms of cation polyhedra. The Ca^{2+}, Ga^{3+}, and Ge^{4+} cations are surrounded by eight, six, and four oxygen anions forming a dodecahedron, an octahedron, and a tetrahedron respectively, as shown in Figure 1b. The doped lanthanide ions prefer to occupy the dodecahedral site of Ca^{2+} in the CGGG host because of the approximate ionic radii between Ca^{2+} (r = 1.12 Å with CN = 8) and Tm^{3+}/Yb^{3+} (Tm^{3+}, r = 0.99 Å; Yb^{3+}, r = 0.98 Å with CN = 8);[33−35] while the doped Cr^{3+} ion is easily portioned into the octahedral site of Ga^{3+} in the CGGG host due to the same ionic radii between Ga^{3+} (r = 0.62 Å with CN = 6) and Cr^{3+} (r = 0.62 Å with CN = 6) as well as the strong ligand-field stabilization energy of Cr^{3+} in 6-fold coordination.[36,37] Actually, the incorporation of lanthanide and transition metal ions into $Ca_3Ga_2Ge_3O_{12}$ host by substituting the Ca^{2+} and Ga^{3+} respectively has been demonstrated previously by electron spin resonance (ESR) spectroscopic analyses as well as optical characterizations.[38,39]

PL excitation (PLE) spectrum of Cr^{3+}:CGGG (Figure 2a) exhibits four broad excitation bands peaking at 260, 311, 458, and 650 nm, respectively. The 260 nm excitation band is ascribed to the absorption of the CGGG host, and the 311, 458, and 650 nm ones are attributed to the $^4A_2 \rightarrow {}^4T_1(^4P)$, $^4A_2 \rightarrow {}^4T_1(^4F)$, and $^4A_2 \rightarrow {}^4T_2(^4F)$ transitions of Cr^{3+}, respectively. The PL spectrum of Cr:CGGG under 458 nm excitation at room temperature (RT) shows a broadband emission in the wavelength range of 650−850 nm originating from the Cr^{3+} $^4T_2 \rightarrow {}^4A_2$ transition, as shown in the dotted curve of Figure 2a. Impressively, several narrow emission bands (assigned to the Cr^{3+} $^2E \rightarrow {}^4A_2$ transition) are superimposed on this broad emission one in the low-temperature (77 K) spectrum, suggesting that the Cr^{3+} ^2E level is close to the Cr^{3+} $^4T_2(^4F)$ one, i.e., Cr^{3+} ions locate in an intermediate crystal-field

dx.doi.org/10.1021/ic501238u | Inorg. Chem. 2014, 53, 8638−8645

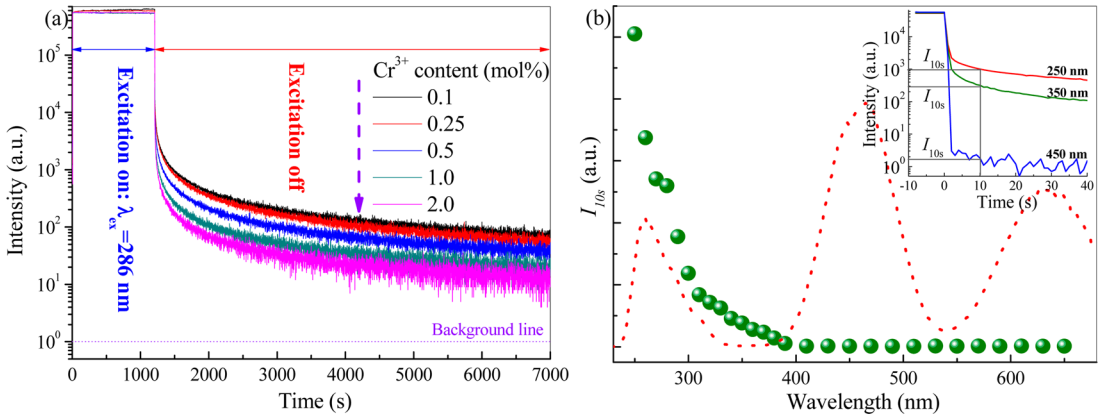

Figure 3. (a) LLP decay curves of Cr:CGGG phosphors doped with various Cr^{3+} contents monitored at 750 nm emission after 286 nm light illumination for 20 min. (b) Afterglow intensity I_{10s} (represented by green balls) as a function of irradiation wavelengths (250−650 nm); insets are LLP decay curves after irradiations at 250, 350, and 450 nm. PLE spectrum (red dotted curve) is also provided as a comparison.

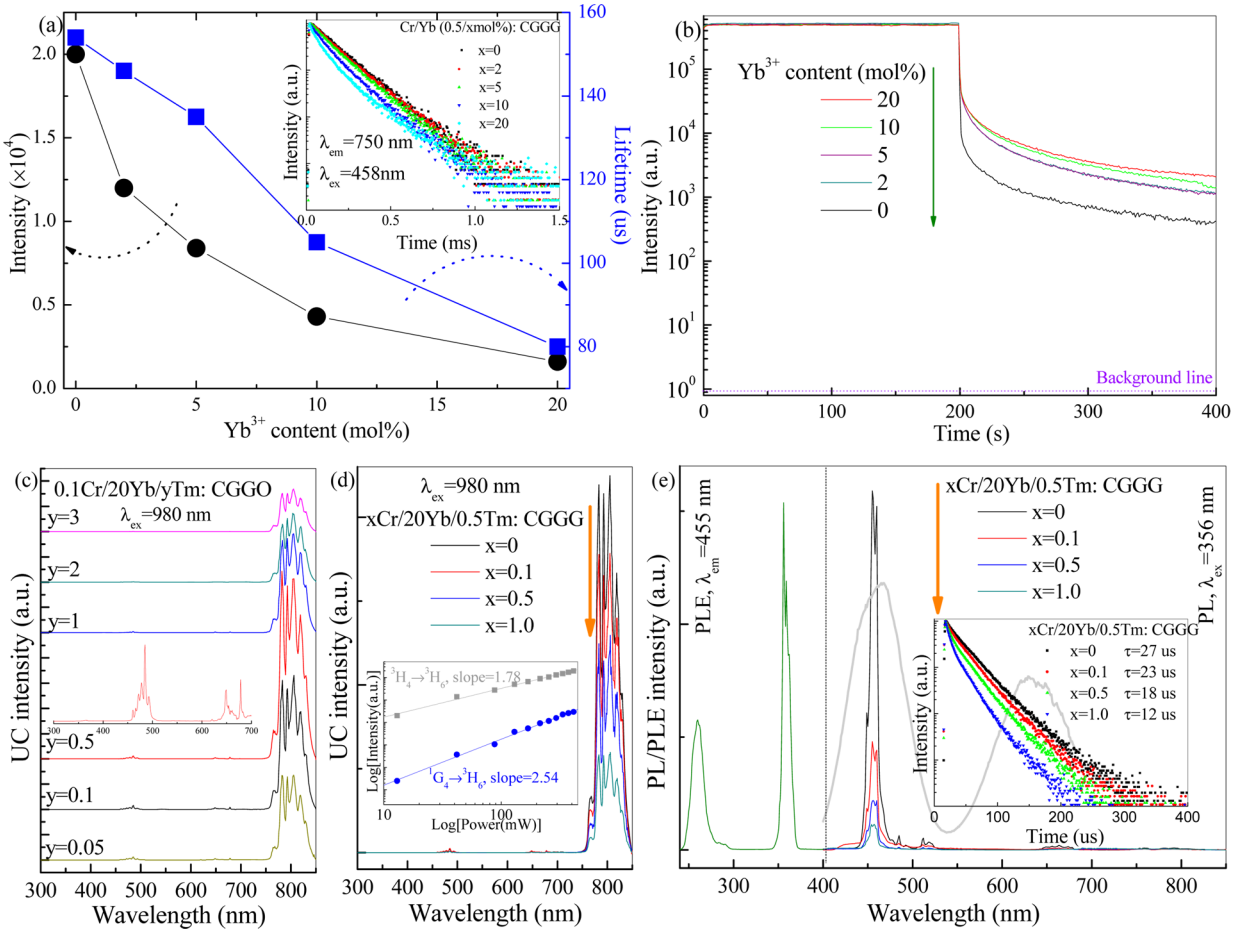

Figure 4. (a) The dependence of emission intensity and lifetime (corresponding to the Cr^{3+} $^4T_2 \rightarrow {}^4A_2$ transition) in Cr/Yb:CGGG on Yb^{3+} doping content; inset shows PL decay curves of 0.5Cr/*x*Yb:CGGG (*x* = 0, 2, 5, 10, and 20 mol %) samples. (b) LLP decay curves of 0.5Cr/*x*Yb:CGGG phosphors after 286 nm light illumination for 200 s. UC emission spectra of (c) *x*Cr/20Yb/0.5Tm (*x* = 0, 0.1, 0.5, and 1.0 mol %) and (d) 0.1Cr/20Yb/*y*Tm (*y* = 0.05, 0.1, 0.5, 1, 2, and 3 mol %) triply doped CGGG samples. Inset of panel c is the enlarged spectrum in the wavelength range of 300−700 nm, and inset of panel d is the log−log plots of UC emission intensity versus NIR excitation power. (e) PLE and PL spectra of *x*Cr/20Yb/0.5Tm:CGGG samples (PLE spectrum for Cr^{3+} 750 nm emission is also provided as a comparison); inset shows PL decay curves of the corresponding samples in panel e.

environment of the CGGG host. Evidently, the radiative decay of the Cr^{3+} spin-allowed $^4T_2 \rightarrow {}^4A_2$ transition (monitored at 750 nm emission at RT) is obviously faster than that of the Cr^{3+} spin-forbidden $^2E \rightarrow {}^4A_2$ transition (monitored at 702 nm emission at 77 K) in Cr:CGGG phosphor (Figure 2b). With increase of Cr^{3+} doping content, the lifetime of the Cr^{3+}:$^4T_2$ state decreases gradually, while the Cr^{3+} luminescence intensifies gradually with Cr^{3+} content increasing from 0.1 to

dx.doi.org/10.1021/ic501238u | Inorg. Chem. 2014, 53, 8638−8645

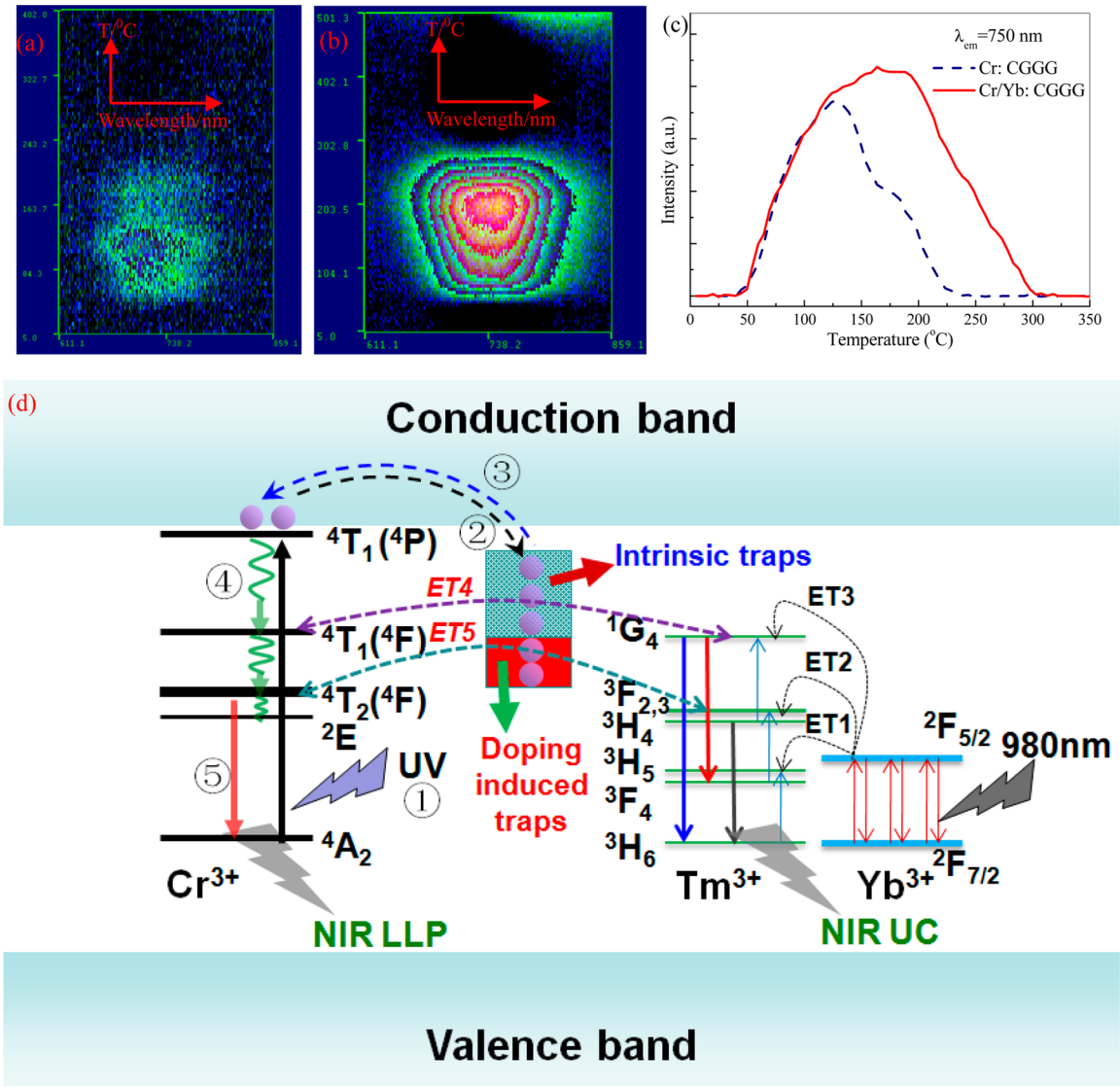

Figure 5. Three-dimensional thermoluminescence spectra of (a) Cr:CGGG and (b) Cr/Yb:CGGG phosphors; (c) thermoluminescence curves of both samples corresponding to 750 nm emission after UV excitation for 5 min; (d) schematic illustration of the NIR LLP and NIR-to-NIR UCL mechanisms in Cr/Yb/Tm:CGGG; the straight-line and dotted-line arrows represent optical transition and electron transfer processes, respectively, and the wave arrows represent nonradiative relaxation.

1.0 mol %, and then weakens with furthering increasing Cr^{3+} content to 2.0 mol %, as revealed in the inset of Figure 2b. Accordingly, the luminescent quantum yield of the 1 mol % Cr^{3+} doped CGGG sample is determined to be 72% (Figure 2c).

As shown in Figure 2d, a Tanabe−Sugano diagram is used to describe a complete level scheme for Cr^{3+} in the CGGG host. The value of the local crystal-field parameter Dq is obtained from the mean peak energy of the $^4A_2 \rightarrow {}^4T_2$ transition:[40]

$$Dq = \frac{E(^4A_2 \rightarrow {}^4T_2)}{10} \quad (2)$$

Moreover, based on the mean peak energies of the $^4A_2 \rightarrow {}^4T_2$ and $^4A_2 \rightarrow {}^4T_1$ transitions, the Racah parameter B can be evaluated from the expression

$$\frac{Dq}{B} = \frac{15(x-8)}{(x^2-10x)} \quad (3)$$

where the parameter x is defined as

$$x = \frac{E(^4A_2 \rightarrow {}^4T_1) - E(^4A_2 \rightarrow {}^4T_2)}{Dq} \quad (4)$$

Based on the experimental data, Dq/B is determined to be 2.35. This intermediate value of the parameter Dq/B for Cr^{3+} in the CGGG host is consistent with the simultaneous presence of the broad and the narrow emission bands at low temperature (77 K) shown in Figure 2a.

Besides the intense and broad NIR PL, the Cr:CGGG phosphors also exhibit NIR LLP after the removal of the excitation source. Figure 3a shows the LLP decays of Cr:CGGG phosphors doped with various Cr^{3+} contents by monitoring 750 nm emission after irradiation by a 286 nm ultraviolet light for 20 min. The data were recorded as a function of LLP intensity versus time, and the recording time lasted for 7000 s. The LLP intensity decreases quickly in the first several seconds and then decays very slowly. After 7000 s of persistent luminescence, the LLP intensity is still high, indicating that the NIR LLP of the present phosphors should

dx.doi.org/10.1021/ic501238u | Inorg. Chem. 2014, 53, 8638−8645

last longer than 7000 s. With increase of Cr^{3+} doping content, the LLP decay becomes faster due to concentration quenching. This is quite different from the case of PL, where there is an optimal Cr^{3+} doping content (1 mol %). Notably, although the NIR PL can be effectively induced by a wide range of excitation wavelength (230−680 nm, Figure 2a), the situation for the NIR LLP should be different because of their different activation mechanisms. To understand the effectiveness of different excitation wavelengths (energies) for NIR LLP, the relationship between LLP intensity and excitation wavelength was studied. As exhibited in the inset of Figure 3b, the LLP decay curves monitored at 750 nm emission under the excitation at different wavelengths between 250 to 650 nm with 10 nm step for 10 min were recorded. To avoid the influence of the early fast decay on the analysis of LLP, the persistent emission intensities recorded 10 s after the stoppage of the irradiation (I_{10s}) were used as the references. Figure 3b shows the persistent intensity I_{10s} of the Cr:CGGG phosphor as a function of the excitation wavelength. The PL excitation spectrum is also presented for comparison. Evidently, the NIR persistent luminescence can be effectively achieved by UV (250−400 nm) illumination, i.e., by exciting electrons into the conduction band of CGGG as well as the $^4T_1(^4P)$ excitation band of Cr^{3+}.

In a further experiment, lanthanide ions were introduced into the Cr:CGGG phosphor to induce upconversion luminescence. First, the impact of Yb^{3+} doping on PL, decay, and LLP of Cr:CGGG was investigated. As revealed in Figure 4a, with increase of Yb^{3+} content in Cr/Yb:CGGG, the decay lifetime corresponding to the Cr^{3+} $^4T_2 \rightarrow {}^4A_2$ transition decreases rapidly, the decay curves turn to be nonexponential, and the Cr^{3+} luminescence monotonously weakens, implying the introducing of the extra decay pathway by Yb^{3+} dopants, i.e., energy transfer from Cr^{3+} to Yb^{3+}. As revealed in Figure S1 in the Supporting Information, PLE and PL spectra of Cr:CGGG and Cr/Yb:CGGG samples confirm the existence of sensitized emission of Yb^{3+} upon excitation into Cr^{3+}. However, the case for long-lasting phosphorescence is quite different. As demonstrated in Figure 4b and Figure S2 in the Supporting Information, the LLP intensity increases with increase of Yb^{3+} doping content, indicating that introducing Yb^{3+} ions into CGGG host is beneficial to long-lasting phosphorescence of Cr^{3+}. Figures 4c and 4d show the UC emission spectra of Cr/Yb/Tm triply doped CGGG samples under 980 nm NIR excitation. All the spectra exhibit the weak blue/red and dominant NIR emission bands of Tm^{3+} originating from the following three transitions: $^1G_4 \rightarrow {}^3H_6$ (478 nm), $^1G_4 \rightarrow {}^3F_4$ (650 nm), and $^3H_4 \rightarrow {}^3H_6$ (800 nm). The optimal Tm^{3+} content is 0.5 mol % with fixed 0.1 mol % Cr^{3+} and 20 mol % Yb^{3+} in CGGG host (Figure 4c). Studies of the power dependence of UC emissions (inset of Figure 4d) reveal that the blue/red emitting state ($^1G_4$) and NIR emitting one ($^3H_4$) are populated via the three- and two-photon processes, respectively. As exhibited in Figure 4d, UC luminescence weakens gradually with increase of Cr^{3+} content, indicating that there is adverse energy transfer from Tm^{3+} to Cr^{3+}. Figure 4e shows the PLE and PL spectra of *x*Cr/20Yb/0.5Tm:CGGG samples. Obviously, with increase of Cr^{3+} content, the Tm^{3+} photoluminescence weakens gradually (Figure 4e) and the lifetime corresponding to the Tm^{3+}:$^1G_4 \rightarrow {}^3H_6$ transition decreases monotonously (inset of Figure 4e), further confirming the existence of energy transfer from Tm^{3+}:$^1G_4$ to Cr^{3+}:$^4T_1(^4F)$. This can be well evidenced by the overlap of Tm^{3+} emission and Cr^{3+} excitation spectra in the Cr/Yb/Tm triply doped sample (Figure 4e).

Defect centers play an essential role for LLP because they can capture free carriers and then immobilize them for an appropriately long period of time. Notably, after UV irradiation, the body color of the Cr:CGGG phosphor changes from green to pink, and the UV irradiation induced coloration can be quickly bleached by heating at 350 °C. This result indicates the formation of photochromic centers probably induced by the trapping of photogenerated electrons by the intrinsic defects (such as Schottky disorder, oxygen vacancy, and antisite defect) in Cr:CGGG.[39,41,42] With introducing Yb^{3+} ions into the CGGG host, Yb^{3+} will replace Ca^{2+} and extra defects should appear in the crystal to compensate for an excessive positive charge. In CGGG, this compensation is provided by excessive Ga^{3+} ions replacing Ge^{4+} ones, i.e., by "anti-structural" defects $Ga_{(d)}{}^{3+}$.[39] In order to investigate the traps in Cr/Yb:CGGG, three-dimensional thermoluminescence spectra of Cr:CGGG and Cr/Yb:CGGG were recorded after UV (286 nm) radiation for 5 min, as shown in Figures 5a and 5b, from which TL curves corresponding to 750 nm emission (Figure 5c) were extracted. The TL curve of Cr:CGGG consists of two broad bands with maxima at 130 and 185 °C, which correspond to the shallow and deep traps, respectively. Obviously, the doping of Yb^{3+} ions into Cr:CGGG makes the TL band broader, i.e., produces another deeper trap near 250 °C. It is worth noting that such an additional deeper trap induced by Ln^{3+} doping can further capture and immobilize free carriers and subsequently improve LLP performance.

Based on the above results and discussion, we propose the mechanisms to account for the NIR LLP and NIR-to-NIR UCL in the Cr/Yb/Tm:CGGG phosphor, as schematically demonstrated in Figure 5d. For UC processes, once the sensitizers (Yb^{3+} ions) are populated with NIR laser excitation, the first energy transfer of Yb^{3+}:$^2F_{5/2}$ + Tm^{3+}:$^3H_6 \rightarrow Yb^{3+}$:$^2F_{7/2}$ + Tm^{3+}:$^3H_5$ (ET 1) takes place. The $^3H_5$ level is then relaxed mainly by a nonradiative de-excitation way, populating the lower lying Tm^{3+}:$^3F_4$ state. Then, the second energy transfer involving Yb^{3+}:$^2F_{5/2}$ + Tm^{3+}:$^3F_4 \rightarrow Yb^{3+}$:$^2F_{7/2}$ + Tm^{3+}:$^3F_{2,3}$ (ET 2) proceeds. The lower lying Tm^{3+}:$^3H_4$ state then receives electrons from the nonradiative relaxation of $^3F_{2,3}$ states, allowing the occurrence of the third energy transfer which populates the Tm^{3+}:$^1G_4$ state via Yb^{3+}:$^2F_{5/2}$ + Tm^{3+}:$^3H_4 \rightarrow Yb^{3+}$:$^2F_{7/2}$ + Tm^{3+}:$^1G_4$ (ET 3).[43] From Tm^{3+}:$^1G_4$ and Tm^{3+}:$^3H_4$ states, weak blue/red emissions originating from $^1G_4 \rightarrow {}^3H_6$, $^3F_4$, and an intense NIR UC one ascribed to a $^3H_4 \rightarrow {}^3H_6$ transition occur. For LLP processes, upon UV (250−400 nm) excitation, the incident photons are absorbed by Cr^{3+} ions, and the ground-state electrons of the Cr^{3+} ions are promoted to the $^4T_1(^4P)$ level localized near the conduction band of the CGGG host (process ①). The excited electrons are subsequently captured by traps through the conduction band (process ②). With a sufficient irradiation time, all of the traps are filled. After the stoppage of irradiation, direct recombination between the conduction electrons (released from the traps) and the Cr^{3+} ions repopulates the Cr^{3+}:$^4T_1(^4P)$ state (process ③). Afterward, nonradiative relaxation of electrons from the Cr^{3+}:$^4T_1(^4P)$ state to $^4T_1(^4F)$ and then to $^4T_2(^4F)$ populates the Cr^{3+}:$^4T_2(^4F)$ state (process ④), from which the NIR broadband LLP occurs (process ⑤).

Notably, the results for the quenching of Cr^{3+} photoluminescence and the enhancing of Cr^{3+} long-lasting phosphorescence upon introducing Yb^{3+} are not contradictory

dx.doi.org/10.1021/ic501238u | Inorg. Chem. 2014, 53, 8638−8645

because of their different activation mechanisms. For Cr^{3+} photoluminescence, the addition of Yb^{3+} into the CGGG host will induce extra energy transfer from Cr^{3+} to Yb^{3+} and subsequently weaken the Cr^{3+} luminescence. In addition, due to energy-level matching between Cr^{3+} and Tm^{3+}, energy transfers between Cr^{3+}:$^4T_1(^4F)$ and Tm^{3+}:$^1G_4$ (ET4) as well as between Cr^{3+}:$^4T_2(^4F)$ and Tm^{3+}:$^3F_{2,3}$ (ET5) easily occur, which result in the weakening of UCL of Tm^{3+} activators. Similarly, the emission quenching phenomena will be observed when adopting Er^{3+} or Ho^{3+} ions as the activators (the results are not shown here). Fortunately, for Cr^{3+} long-lasting phosphorescence, the introduce of Yb^{3+} into the CGGG host by substituting Ca^{2+} ones will induce extra deeper traps due to the requirement of charge balance, which are beneficial to capturing free carriers and then immobilizing them for a longer period of time and subsequently increasing the afterglow time of Cr^{3+}. As a consequence, doping low Cr^{3+}/Tm^{3+} contents and high Yb^{3+} one into the CGGG host (for example, 0.1 mol % Cr/20 mol % Yb/0.5 mol % Tm:CGGG) is favorable to the realization of both efficient NIR LLP and NIR UCL.

4. CONCLUSION

In summary, we have successfully fabricated a NIR long-persistent and NIR upconversion bifunctional Cr/Yb/Tm:$Ca_3Ga_2Ge_3O_{12}$ phosphor with afterglow time lasting for more than 7000 s. The doped Cr^{3+} ions prefer to occupy the octahedral site of Ga^{3+} with the intermediate crystal-field strength, while the Yb^{3+}/Tm^{3+} ions incorporate into the dodecahedral site of Ca^{2+}. The NIR LLP can be effectively realized by UV (250−400 nm) illumination, but is hardly achieved by visible light (400−650 nm) irradiation. The filling/releasing of electrons into/from the intrinsic traps of $Ca_3Ga_2Ge_3O_{12}$ through the conduction band of host are proposed to be responsible for the realization of the NIR LLP in Cr^{3+} single doped sample. Impressively, the addition of lanthanide ions into Cr:$Ca_3Ga_2Ge_3O_{12}$ can greatly increase the Cr^{3+} afterglow time due to the formation of extra deeper traps. Notably, to realize the application of the present bifunctional phosphors in sensitive bioassay, many efforts, such as reducing size into nanoscale, controlling morphology, conjugating biomolecules on crystal surfaces, performing measurements in vitro as well as in vivo, and so on, are still needed to be carried out in the future.

■ ASSOCIATED CONTENT

Supporting Information

PLE and PL spectra of Cr:CGGG and Cr/Yb:CGGG samples (Figure S1). Long-lasting phosphorescent spectra of various Cr/Yb codoped CGGG samples (Figure S2). This material is available free of charge via the Internet at http://pubs.acs.org.

■ AUTHOR INFORMATION

Corresponding Author

*E-mail: dqchen@hdu.edu.cn. Tel/fax: 0086-571-87713542.

Notes

The authors declare no competing financial interest.

■ ACKNOWLEDGMENTS

This work was supported by the National Natural Science Foundation of China (21104068, 21271170), the Natural Science Foundation of Fujian for Distinguished Young Scholars (2012J06014), the Educational Commission of Zhejiang Province of China (Y201121238), and Zhejiang province public welfare project (2012C23098). The authors thank Prof. Yuansheng Wang and Ju Xu of Fujian Institute of Research on the Structure of Matter for the measurements of photoluminescence spectra and decay curves, and Prof. Jing Wang and Dr. Ye Li of Sun Yat-Sen University for the measurements of three-dimensional thermoluminescence spectra.

■ REFERENCES

(1) Weissleder, R.; Pittet, M. J. *Nature* **2008**, *452*, 580−589.
(2) Hellebust, A.; Richards-Kortum, R. *Nanomedicine* **2012**, *7*, 429−445.
(3) Yan, J.; Estévez, M. C.; Smith, J. E.; Wang, K.; He, X.; Wang, L.; Tan, W. *Nano Today* **2007**, *2*, 44−50.
(4) Hong, G.; Robinson, J. T.; Zhang, Y.; Diao, S.; Antaris, A. L.; Wang, Q.; Dai, H. *Angew. Chem., Int. Ed.* **2012**, *51*, 9818−9821.
(5) Dreaden, E. C.; Alkilany, A. M.; Huang, X.; Murphy, C. J.; EI-Sayed, M. A. *Chem. Soc. Rev.* **2012**, *41*, 2740−2779.
(6) Wang, F.; Liu, X. G. *Chem. Soc. Rev.* **2009**, *38*, 976−989.
(7) Abdukayum, A.; Chen, J. T.; Zhao, Q.; Yan, X. P. *J. Am. Chem. Soc.* **2013**, *135*, 14125−14133.
(8) Auzel, F. *Chem. Rev.* **2004**, *104*, 139−174.
(9) Haase, M.; Schäfer, H. *Angew. Chem., Int. Ed.* **2011**, *50*, 5808−5829.
(10) Nyk, M.; Kumar, R.; Ohulchanskyy, T. Y.; Bergey, E. J.; Prasad, P. N. *Nano Lett.* **2008**, *8*, 3834−3838.
(11) Zhou, J.; Liu, Z.; Li, F. Y. *Chem. Soc. Rev.* **2012**, *41*, 1323−1349.
(12) Liu, Y. S.; Tu, D. T.; Zhu, H. M.; Chen, X. Y. *Chem. Soc. Rev.* **2013**, *42*, 6924−6958.
(13) Naccache, R.; Chevallier, P.; Lagueux, J.; Gossuin, Y.; Laurent, S.; Elst, L. V.; Chilian, C.; Capobianco, J. A.; Fortin, M. *Adv. Healthcare Mater.* **2013**, *2*, 1478−1488.
(14) Li, C. X.; Lin, J. *J. Mater. Chem.* **2010**, *20*, 6831−6847.
(15) Gai, S. L.; Li, C. X.; Yang, P. P.; Lin, J. *Chem. Rev.* **2014**, *114*, 2343−2389.
(16) Van den Eeckhout, K.; Smet, P. F.; Poelman, D. *Materials* **2010**, *3*, 2536−2566.
(17) le Masne de Chermont, Q.; Chaneac, C.; Seguin, J.; Pelle, F.; Maitrejean, S.; Jolivet, J. P.; Gourier, D.; Bessodes, M.; Scherman, D. *Proc. Natl. Acad. Sci. U.S.A.* **2007**, *104*, 9266−9271.
(18) Rodríguez Burbano, D. C.; Martín Rodríguez, E.; Dorenbos, P.; Bettinelli, M.; Capobianco, J. A. *J. Mater. Chem. C* **2014**, *2*, 228−231.
(19) Li, Y.; Zhou, S. F.; Li, Y. Y.; Sharafudeen, K.; Ma, Z. J.; Dong, G. P.; Peng, M. Y.; Qiu, J. R. *J. Mater. Chem. C* **2014**, *2*, 2657−2663.
(20) Pan, Z. W.; Lu, Y. Y.; Liu, F. *Nat. Mater.* **2012**, *11*, 58−63.
(21) Liu, F.; Yan, W. Z.; Chuan, Y. J.; Zhen, Z. P.; Xie, J.; Pan, Z. W. *Sci. Rep.* **2013**, *3*, 1554.
(22) Weissleder, R. *Nat. Biotechnol.* **2001**, *19*, 316−317.
(23) Chen, G. Y.; Ohulchanskyy, T. Y.; Kumar, R.; Ågren, H.; Prasad, P. N. *ACS Nano* **2010**, *4*, 3163−3168.
(24) Chen, D. Q.; Yu, Y. L.; Huang, F.; Lin, H.; Huang, P.; Yang, A. P.; Wang, Z. X.; Wang, Y. S. *J. Mater. Chem.* **2012**, *22*, 2632−2640.
(25) Martín-Rodríguez, R.; Valiente, R.; Rodríguez, F.; Bettinelli, M. *Nanotechnology* **2011**, *22*, 265707.
(26) Zhuang, Y.; Ueda, J.; Tanabe, S. *Appl. Phys. Express* **2013**, *6*, 052602.
(27) Bessière, A.; Jacquart, S.; Priolkar, K.; Lecointre, A.; Viana, B.; Gourier, D. *Opt. Express* **2011**, *19*, 10131−10137.
(28) Xu, J.; Chen, D. Q.; Yu, Y. L.; Zhu, W. J.; Zhou, J. C.; Wang, Y. S. *Chem.—Asian J.* **2014**, *9*, 1020−1025.
(29) Hu, L. Y.; Yan, B.; Zhang, J. H.; Wang, X. J. *J. Phys. D: Appl. Phys.* **2007**, *40*, 7519−7522.
(30) Hyppänen, I.; Hölsä, J.; Kankare, J.; Lastusaari, M.; Pihlgren, L. *J. Nanomater.* **2007**, *2007*, 16391.
(31) Zhang, R.; Lin, H.; Yu, Y. L.; Chen, D. Q.; Xu, J.; Wang, Y. S. *Laser Photonics Rev.* **2014**, *8*, 158−164.
(32) Damen, J. P. M.; Pistorius, J. A.; Robertson, J. M. *Mater. Res. Bull.* **1977**, *12*, 73−78.

(33) Shannon, R. D.; Prewitt, C. T. *Acta Crystallogr.* **1969**, *B25*, 925−946.
(34) Shannon, R. D.; Prewitt, C. T. *Acta Crystallogr.* **1970**, *B26*, 1046−1048.
(35) Shannon, R. D. *Acta Crystallogr.* **1976**, *A32*, 751−767.
(36) Viana, B.; Lejus, A. M.; Vivien, D.; Poncon, V.; Boulon, G. *J. Solid State Chem.* **1987**, *71*, 77−86.
(37) Singh, V.; Chakradhar, R. P. S.; Rao, J. L.; Kim, D. K. *Solid State Sci.* **2008**, *10*, 1525−1532.
(38) Moraes, I. J.; de Souza, R. R.; do Nascimento, O. R.; Terrile, M. C.; Barberis, G. E. *Solid State Commun.* **1995**, *95*, 251−254.
(39) Kostyk, L. V.; Nosenko, A. E.; Kravchishin, V. V. *Opt. Spectrosc.* **1997**, *82*, 548−551.
(40) Casalboni, M.; Luci, A.; Grassano, U. M.; Mill, B. V.; Kaminskii, A. A. *Phys. Rev. B* **1994**, *49*, 3781−3790.
(41) Nosenko, A. E.; Kostyk, L. V. *Radiat. Prot. Dosim.* **1996**, *65*, 127.
(42) Kanai, T.; Satoh, M.; Miura, I. *J. Am. Ceram. Soc.* **2008**, *91*, 456−462.
(43) Chen, D. Q.; Wang, Y. S.; Yu, Y. L.; Huang, P. *Appl. Phys. Lett.* **2007**, *91*, 051920.